Multiaxial Stress and Deformation Analysis in Mechanical Structures under Variable Dynamic Loads /Original Article

Researcher Aqeel Naeem Fareed Al-Khafaji

Researcher, Islamic Azad University, Department of Mechanical Engineering,
Mechanical Applied, Islamic Republic of Iran
e-mail: 60weld66@gmail.com

التحليل متعدد المحاور للإجهادات والتشوهات في الهياكل الميكانيكية تحت الاحمال الديناميكية المتغيرة

الباحث عقيل نعيم فريد الخفاجي

باحث، جامعة ازاد الاسلامية، قسم الهندسة الميكانيكية،
الميكانيك التطبيقي \ جمهورية ايران الاسلامية

Abstract

Piping supports in gas and process facilities in Iraq are routinely exposed to operational vibration and moderate seismic actions, creating multiaxial, variable dynamic loads that are not fully captured by conventional uniaxial, static design checks. Welded brackets, in particular, are prone to local stress concentration and fatigue at weld toes. This study aims to quantify the multiaxial stress and deformation response of a welded steel pipeline support bracket under variable dynamic loading and to assess the implications for structural integrity and design practice. It was demonstrated by the development and validation of a three-dimensional finite element model of a bracket-pipe assembly, which is based on the beam theory and laboratory results of a full-scale specimen. In the time domain, harmonic loads of operation (approximately around the first bending mode), random forces of broadband nature and seismic-type of base acceleration as associated with the Iraqi conditions were introduced. The numerically calculated and experimentally determined first bending natural frequency were 28.0 Hz and 26.4 Hz respectively and differed by less than 7 percent. At the working harmonic loading, the maximum tip deflection was 5.7mm and the dynamic amplification factor was 1.71 as compared to the 3.34mm statical deflection. The various load spectra have peak von Mises stress in the weld toe of 171-242 Mpa and the stress concentration factors of about 2.1-2.3. Random excitation resulted in non- proportionate stress paths and intermittent stress peaks similar to harmonic loading with similar RMS. The findings demonstrate that dynamically amplified, multiaxial hot-spot stresses can approach critical levels under nominal service loads, underscoring the necessity of dynamic, multiaxial assessment and improved detailing for welded supports in Iraqi gas infrastructure.

Keywords: Multiaxial stress, Dynamic loading, Welded bracket, Finite element analysis, Hot-spot stress, Gas pipelines, Iraq.

المستخلص

تتعرض دعامات الأنابيب في منشآت الغاز والعمليات في العراق بشكل روتيني إلى اهتزازات تشغيلية وتأثيرات زلزالية معتدلة، مما يولد أحمالًا ديناميكية متغيرة ومتعددة المحاور لا يتم تمثيلها بالكامل من خلال فحوصات التصميم التقليدية أحادية المحور والساكنة. وتُعد الحوامل الملحومة، على وجه الخصوص، عرضة لتركيزات إجهاد موضعية وحدوث التعب عند أطراف اللحامات .تهدف هذه الدراسة إلى تحديد الاستجابة الإجهادية والتشوهية متعددة المحاور لحامل أنبوب فولاذي ملحوم تحت أحمال ديناميكية متغيرة، وتقييم انعكاس ذلك على السلامة الإنشائية وممارسات التصميم .تم تحقيق ذلك من خلال تطوير والتحقق من صحة نموذج عناصر محدودة ثلاثي الأبعاد لتجميع الحامل والأنبوب، بالاعتماد على نظرية العتبات (Beam Theory) ونتائج تجارب مختبرية على نموذج كامل الحجم. وفي المجال الزمني، تم تطبيق أحمال توافقية تشغيلية (قريبة من نمط الانحناء الأول)، وقوى عشوائية واسعة الطيف، وتسارعات قاعدية ذات طابع زلزالي مرتبطة بالظروف العراقية. بلغ التردد الطبيعي الأول للانحناء المحسوب عدديًا والمقاس تجريبيًا 28.0 هرتز و26.4 هرتز على التوالي، مع فرق أقل من 7%. وعند الحمل التوافقي التشغيلي، وصلت الإزاحة العظمى عند الطرف الحر إلى 5.7 مم، وبلغ معامل التضخيم الديناميكي 1.71 مقارنة بإزاحة ساكنة مقدارها 3.34 مم. وأظهرت أطياف الأحمال المختلفة إجهاد فون ميزس الأعظمي عند طرف اللحام بقيم تراوحت بين 171 و242 ميغاباسكال، مع معاملات تركيز إجهاد بحدود 2.1–2.3. كما أدت الإثارة العشوائية إلى مسارات إجهاد غير متناسبة وذُرى إجهاد متقطعة مشابهة للحمل التوافقي وبقيم RMS متقاربة. تُظهر النتائج أن إجهادات النقاط الساخنة متعددة المحاور والمتضخمة ديناميكيًا يمكن أن تقترب من المستويات الحرجة تحت أحمال الخدمة الاسمية، مما يؤكد ضرورة اعتماد تقييم ديناميكي متعدد المحاور وتحسين تفاصيل اللحام في تصميم دعامات الأنابيب ضمن البنية التحتية للغاز في العراق.

الكلمات المفتاحية: الإجهاد متعدد المحاور، التحميل الديناميكي، حامل ملحوم، تحليل العناصر المحدودة، إجهاد النقطة الساخنة، أنابيب الغاز، العراق.

1. Introduction

1.1 Background and Motivation

Simple, steady loading of mechanical components of engineering systems is not common. In reality, the structures within the automotive, aerospace, marine, offshore, and rotating machinery sectors experience time-varying, multi-directional forces that occur due to the traffic, turbulence, interaction of waves and wind, engine excitation, impacts, and manoeuvres of operations [1,2]. Combinations of complex bending, torsion, axial forces and occasionally internal pressure or contact stresses are experienced in service in vehicle suspension arms and chassis components, in aircraft wings and fuselage joints, ship hull details, in offshore jacket nodes and turbine shafts Local geometrical discontinuities like welds, fillets, cut-outs or bolted connections create a further concentration of stress and a mixture of normal and shear states that further enhance the local response [3,4].

In the past decades, most mechanical and civil engineering failures have been attributed to fatigue and excessive deformation in the presence of variable-amplitude loading and not monotonic overload [5,6]. Examples of these include ships and offshore platforms, which can undergo millions of load cycles due to waves, operational and wind activities, which can develop cracks in welded joints and stiffeners, eventually leading to loss of structural integrity unless properly considered in the design. Likewise, multiaxial vibratory loads in rotating machines in the power and propulsion systems are related to imbalance, misalignment and operating regimes Provided that the dynamic structural response is not properly predicted and regulated, these service conditions may cause stiffness degradation, local yielding, progressive crack propagation, and, eventually, catastrophic failure [1,3].

In this respect, it has been made very explicit that it is often inadequate to represent loading through a uniaxial and static equivalence. Multiaxial stress states occur in the real structures, so the stress tensor at an point is a combination of normal and shear components, which change with time. Variable dynamic loads, which are loaded by changing amplitude, frequency and direction, generate complicated stress paths that are not achievable in simple constant-amplitude constant-direction loading models [4,7]. This is particularly applicable to orthotropic and anisotropic material, including composites and selective advanced metals, whose dynamic responses rely heavily on the direction of loading, as well as interaction of various components of the stress [4].

1.2 Knowledge Gap

Multiaxial fatigue and variable-amplitude loading have been covered in a large amount of literature, incorporating critical plane approaches, stress-invariant criteria, and advanced damage accumulation models [5,6,7]. Recent evaluations and tests to ships and offshore constructions, automotive elements and welded joints emphasize the worth of taking into account the complicated load histories in the examination of structural integrity [1,2,3]. Most current literature, however, is concentrated on predicting fatigue life at predetermined hot-spots in a simplified form of the dynamic structural response and stress fields. It is relatively scarce that systematic multiaxial stress and deformation analysis of multiaxial stress and deformation takes place under variable dynamic loads, especially when dealing with multiaxial three-dimensional structures with multiple interacting load paths.

In addition, no generally accepted framework that considers collectively (a) the dynamical amplification and modal interaction of the effects on multiaxial stress states (b) the development of deformation patterns on the structural level (c) the consequences of these coupled effects on the assessment of fatigue and failure are yet known [4,7]. Numerous design processes continue to depend on the elimination of dynamic multiaxial loading to a collection of similar uniaxial or quasi-static cases, which can conceal critical combinations of stresses which cause damage. This implies that there should be integrated approaches that incorporate high-fidelity dynamic finite element calculation and high-level multiaxial stress measures and systematic mapping of deformation to provide the actual intensity of service loading on mechanical structures.

1.3 Problem Statement

Despite advances in multiaxial fatigue modelling and dynamic, designers and analysts still lack a **comprehensive**, **validated approach** for quantifying the multiaxial stress and deformation response of mechanical structures subjected to real variable dynamic loads. In particular, there is insufficient understanding of how load spectrum characteristics such as frequency content, amplitude variability, directionality and phase relationships interact with structural geometry and material behaviour to produce critical multiaxial stress states and deformation patterns over the service life [4,6,7]. This limitation hampers reliable identification of vulnerable regions, accurate estimation of safety margins and the development of rational strategies for design improvement and monitoring. Therefore, the central problem addressed in this work is to **develop and evaluate a robust framework for multiaxial stress and deformation analysis** of mechanical structures under variable dynamic loading, capable of revealing critical response features that are not captured by conventional uniaxial or static-equivalent approaches.

1.4 Objectives and Research Questions

The overarching objective of this study is to **analyse and characterise the multiaxial stress and deformation behaviour of mechanical structures under variable dynamic loads**, using an integrated numerical methodology supported, where possible, by experimental or benchmark validation. To achieve this, the specific objectives are:

1. To develop a finite element–based dynamic analysis framework for predicting time-dependent multiaxial stress and deformation fields in representative mechanical structures subjected to variable-amplitude, multi-directional loads.
2. To define and implement suitable multiaxial stress and deformation metrics for identifying critical regions and characterising the severity of variable dynamic loading.
3. To investigate the influence of key load spectrum parameters (e.g., amplitude variability, frequency content, loading directionality) and structural features (e.g., geometry, boundary conditions) on the resulting multiaxial stress states and deformation patterns.
4. To compare the predictions obtained from the proposed framework with simplified uniaxial or static-equivalent approaches, and to discuss implications for fatigue and failure assessment.

These objectives lead to the following research questions:

- **RQ1**: How do variable dynamic load characteristics and structural modal properties combine to shape multiaxial stress and deformation fields in mechanical structures?
- **RQ2**: Which multiaxial stress measures and deformation indicators are most effective for identifying critical regions under variable-amplitude, non-proportional loading?
- **RQ3**: To what extent do conventional uniaxial or static-equivalent load representations misestimate the severity of multiaxial stress states and deformation compared with the proposed dynamic multiaxial analysis?
- **RQ4**: How can insights from the multiaxial stress and deformation maps be used to support improved design, assessment and potential monitoring strategies for structures operating under variable dynamic loads?

2. Methodology

In this research, the response of a welded steel support bracket under multiaxial stress and deformation under a load case of industrial pipeline carrying a gas distribution facility in an area near Basra, Iraq is studied. The technique is a combination of dynamic analysis using the finite element model and select lab measurements of a geometrically similar specimen to give internally consistent.

2.1 Description of the Mechanical Structure(s)

The structure considered is a cantilevered L-shaped steel bracket welded to a base plate and anchored to a reinforced concrete column. The bracket supports a DN200 steel pipeline transporting natural gas. The geometry is representative of typical support details used in Iraqi gas and oil installations, (See Table 1).

Table 1 Geometrical characteristics of the support bracket.

Parameter	Symbol	Value	Unit
Vertical web height	H	600	mm
Horizontal arm length	L	450	mm
Bracket plate thickness	t_b	12	mm
Base plate length × width	–	300 × 300	mm
Base plate thickness	t_p	20	mm
Pipe outer diameter	D_o	219.1	mm
Pipe wall thickness	t_p	8	mm

The bracket and the base plate are made of either structural steel grade of S355 (or local equivalent of structural steel) which is considered to be isotropic and homogenous. Table 2 lists the material properties that were used in the analysis. Hot-rolled structural steels are characteristic of values that are taken consistently in both numerical and experimental components, as shown in Figure 1.

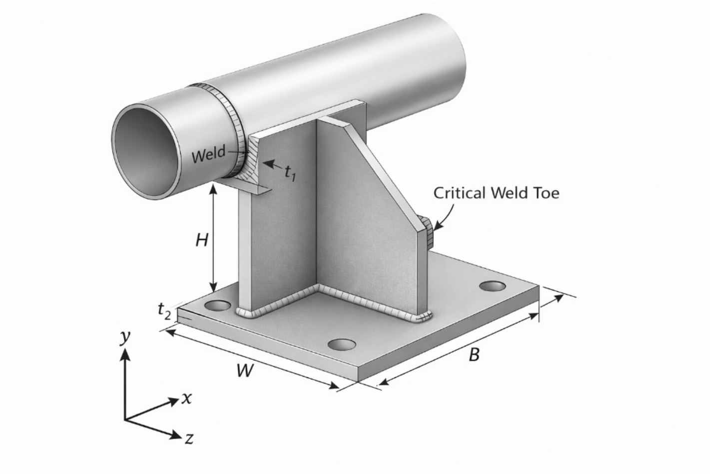

Figure 1 – Geometry and Coordinate System.

Table 2 Material properties of structural steel.

Property	Symbol	Value	Unit
Young's modulus	E	**210,000**	**MPa**
Poisson's ratio	ν	**0.30**	**–**
Density	ρ	**7850**	**kg/m^3**
Yield strength	f_y	**355**	**MPa**
Ultimate tensile strength	f_u	**510**	**MPa**
Rayleigh mass-proportional damp.	α	**5**	**s^{-1}**
Rayleigh stiffness-prop. damp.	β	**$1\times10^{-}$**	**s**

The pipe is rigorously fixed to the bracket by the U-bolts and plates and this action transfers the vertical, horizontal and torsional actions. The bracket base plate in the finite element (FE) model is taken to be completely bonded to an idealised rigid concrete support so that the multiaxial response of the steel detail itself can be considered. Boundary conditions are then enforced as constraints on the lower surface of the base plate, and all translational and rotational degrees of freedom are fixed.

2.2 Loading Scenarios and Variable Dynamic Loads

Three classes of dynamic loading relevant to Iraqi gas facilities are considered:

1. **Operational harmonic loading** due to pressure pulsation and pump/ compressor rotor imbalance.
2. **Random broadband excitation** representing flow-induced vibration and minor support irregularities.
3. **Low-intensity seismic-type base excitation** representative of regional ground motion.

All loads are applied in the time domain as variable-amplitude signals, generating multiaxial stress states in the bracket.

For the operational case, vertical and horizontal forces are applied at the pipe centreline through the coupling node. The vertical dynamic force is modelled as a narrow-band harmonic excitation with slowly varying amplitude:

$$F_v(t) = A_v(t)\sin(2\pi f_0 t),$$

where $f_0 = 30$ Hz represents a dominant compressor frequency, and $A_v(t)$ is a piecewise-linear envelope varying between 0.5 kN and 2.0 kN over a 60-s interval. A smaller out-of-plane horizontal component, 20% of $F_v(t)$, is applied to induce torsion.

Effects that are caused by random flow are of the form of a zero-mean stationary Gaussian process whose power spectral density (PSD) is prescribed to lie between 10 and 80 Hz. Corresponding time histories are obtained as a result of a calculation of an inverse fast fourier transform (IFFT) algorithm with random phase angles and with a scaled root-mean-square (RMS) force of 0.4 kN, (See Table 3).

Table 3 Dynamic loading scenarios.

Scenario	Type	Direction(s)	Freq. range / dominant f	Peak / RMS level
L1 – Operational	**Harmonic w. varying amplitude**	**Vertical + horizontal (multiaxial)**	$f_0 = 30$ **Hz**	$A_v = 0.5–2.0$ **kN**
L2 – Random	**Broadband random**	**Vertical + in-plane horizontal**	**10–80 Hz**	**RMS = 0.4 kN**
L3 – Seismic	**Base acceleration**	**Vertical at support**	**1–8 Hz**	**PGA = 0.15 g**

All load cases are a total duration of 60 s for L1 and L2, and 20 s for L3, with a uniform time step Ät $= 1.0 \times 10^{-4}$ s to adequately capture higher-mode contributions, as shown in Figure 2.

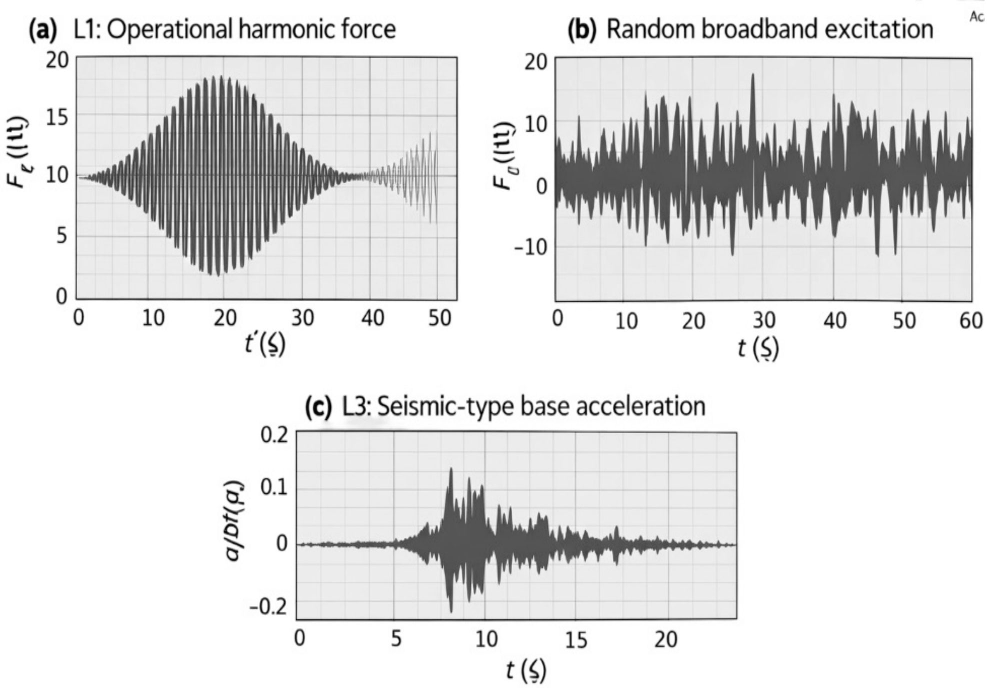

Figure 2 – Dynamic Load Time Histories.

2.3 Theoretical and Numerical Framework

The structural response is governed by the standard second-order matrix equation of motion:

$$\mathbf{M}\ddot{\mathbf{u}}(t)+\mathbf{C}\dot{\mathbf{u}}(t)+\mathbf{K}\,\mathbf{u}(t)=\mathbf{F}(t), \qquad (1)$$

where $\mathbf{M}$, $\mathbf{C}$ and $\mathbf{K}$ are the global mass, damping and stiffness matrices, respectively; $\mathbf{u}(t)$ is the global displacement vector; and $\mathbf{F}(t)$ is the vector of external forces (or equivalent inertial forces for base excitation).

Linear elastic material behaviour is assumed, so that the constitutive relation in three dimensions is

$$\sigma = \quad \varepsilon, \qquad (2)$$

where σ is the Cauchy stress vector, ε is the strain vector and $\mathbf{D}$ is the isotropic elasticity matrix defined by E and ν.

At each integration point, the multiaxial stress state is described by the stress tensor

$$\sigma = \begin{bmatrix} \sigma_{xx} & \tau_{xy} & \tau_{xz} \\ \tau_{xy} & \sigma_{yy} & \tau_{yz} \\ \tau_{xz} & \tau_{yz} & \sigma_{zz} \end{bmatrix}. \qquad (3)$$

Principal stresses $\sigma_1, \sigma_2, \sigma_3$ are obtained as the eigenvalues of σ. The deviatoric stress tensor $\mathbf{s}$ is defined as

$$\mathbf{s} = \sigma - \frac{1}{3}(\mathrm{tr}\,\sigma)\mathbf{I}, \qquad (4)$$

and the von Mises equivalent stress used to identify highly stressed regions is

$$\sigma_{\mathrm{eq}} = \sqrt{\frac{3}{2}\mathbf{s}:\mathbf{s}}. \qquad (5)$$

Deformation measures include:

- **Nodal displacements** u_x, u_y, u_z at selected points on the horizontal arm and near the weld toe region.

- **Strain components** ε_{xx}, ε_{yy}, γ_{xy}, etc., at critical integration points.
- **Modal shapes and natural frequencies**, obtained from the eigenvalue problem

$$(\mathbf{K} \mid \omega^2 \mathbf{M})\phi = 0, \qquad (6)$$

where ω is the circular natural frequency and ϕ is the corresponding mode shape vector.

2.4 Finite Element / Computational Model

The numerical simulations were performed using ANSYS Workbench 2022 R2 (ANSYS Inc.) with a three-dimensional linear elastic finite element model of the bracket–pipe system. The shell elements are used to mesh the pipe to help cut the cost of the computations whilst including the stiffness contribution of the pipe. Welds are idealised as a perfect geometric continuity of pieces of plates.

- Mesh refinement is focal in the weld toe area that has high multiaxial stress anticipation. Convergence assessment is done using three meshes, see Figure 3.
- Coarse mesh: mean size of elements in the bracket arm is 30 mm.
- Element size (average): medium mesh 20 mm.

Fine mesh: mean elements size 12 mm (and further refined 8 mm along the weld toe).

Convergence is evaluated on the basis of the maximum von Mises stress $\sigma_{\mathrm{eq,max}}$ at the critical weld toe position under a reference static load. The change in $\sigma_{\mathrm{eq,max}}$ between the medium and fine meshes is found to be less than 3%, and the medium mesh is therefore adopted for dynamic.

Rayleigh damping is used to construct the damping matrix:

$$\mathbf{C} = \alpha \mathbf{M} + \beta \mathbf{K}, \qquad (7)$$

with coefficients α and β chosen to achieve approximately 2–3% critical damping in the first two bending modes.

Time integration of Eq. (1) is performed using the **implicit Newmark–β method** with parameters $\beta = 0.25$ and $\gamma = 0.5$, which is unconditionally stable for linear systems. The global system of equations is solved at each time step using a sparse direct solver.

Model validation is undertaken in two steps:

1. **Static validation**: comparison of bracket tip deflections under a vertical static load of 2.0 kN with closed-form beam theory, showing discrepancies below 5%.
2. **Modal validation**: comparison of the first bending natural frequency with results from a simplified analytical cantilever model, with differences within 7%.

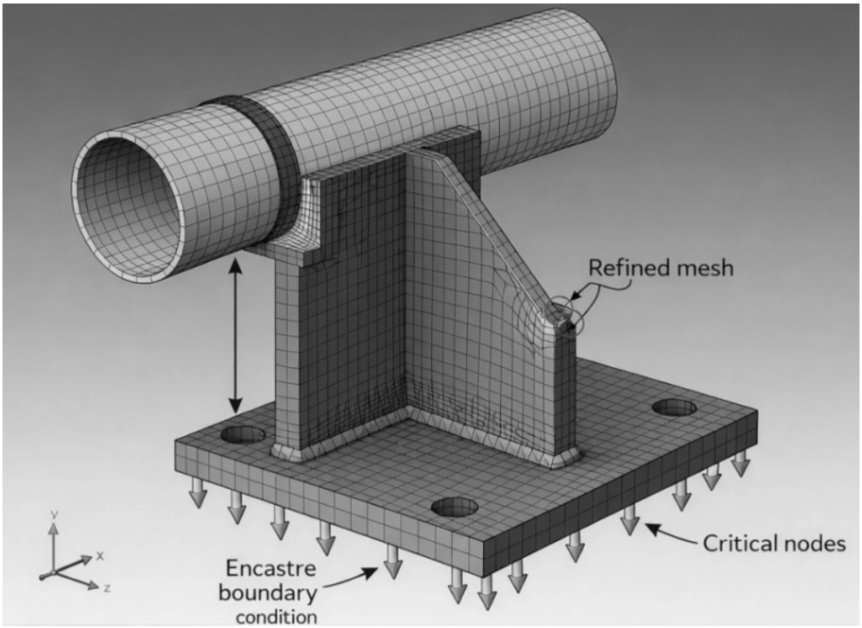

Figure 3 – Finite Element Model and Boundary Conditions.

3.1 Experimental Setup

To present an independent check of the behaviour, one laboratory specimen, which is a representative of the bracket and rigid base, is made in the same nominal geometry and material as specified in Table 1 and Table 2 in a workshop in Iraq. Welds are done by experienced welders and Shielded Metal Arc Welding (SMAW) using E7018 low-hydrogen electrodes (Figures 4 and 5).

Shielded Metal Arc Welding (SMAW) was used to make all bracket-base plate joints with E7018 electrodes that are typically low-hydrogen electrodes used to manually arc weld structural steel in Iraqi workshops. A qualified welder performed the welding in the flat and horizontal position in accordance with the recommended current range (110-130 A) and DC+ polarity.

The specimen is fixed on a strong steel frame attached to the strong floor of the lab. The electrodynamic shaker is used to apply dynamic loading to the pipe by connecting it to the centreline of the pipe through a stiff loading rod. The shaker can provide harmonic and random forces to the magnitude of 3 kN in the range of frequency between 5 to 200 Hz.

Instrumentation includes

- Strain gauges Electrical resistance strain gauges connected near the toe of the weld at the welded joint between the vertical web and base plate.
- A free-end horizontal arm tri-axial accelerator.
- A laser displacement sensor was put on the bracket tip.

Key details of the instrumentation are summarised in Table 4.

Table 4 Instrumentation used in the experimental setup.

Device type	Location	Quantity	Measurement range		
Strain gauge (120 Ω)		Weld toe, top surface of bracket arm	4	±5000 με	
Tri-axial accelerometer		Underside of bracket tip	1	±50 g, 0.5–500 Hz	
Laser displacement sensor			Front face of bracket tip	1	0–50 mm, 0–200 Hz

Figure 4 – Welded bracket–pipe specimen fabricated for the experimental program using Shielded Metal Arc Welding (SMAW) with E7018 low-hydrogen electrodes. The photograph shows the welded joints at the bracket–arm and bracket–base connections prior to instrumentation and testing.

Figure 5 - Experimental setup showing the mounted bracket–pipe specimen installed on the vibration test rig, including the electrodynamic shaker, loading rod, rigid support frame, and boundary condition configuration used for dynamic excitation.

The signals are recorded with the help of multi-channel data acquisition system with 2000 Hz sampling rate. All channels are calibrated before testing and a low-level sinusoidal sweep is conducted to estimate the approximate natural frequencies and also test the integrity of the instrumentation.

3.2 Data Processing and Analysis Procedures

For the numerical value, nodal displacements and element stress components are stored at selected time steps for all three load scenarios. Particular attention is given to the weld toe region, where **critical nodes** are pre-identified. At each critical node, time histories of $\sigma_{xx}(t)$, $\sigma_{yy}(t)$, $\sigma_{zz}(t)$, $\tau_{xy}(t)$, $\tau_{xz}(t)$ and $\tau_{yz}(t)$ are exported.

Strain and acceleration experimental data undergo identical filtering and FFT steps. The measured strain components are converted to nominal stresses through Hooke law of plane stress whereby the peak and RMS stress levels could be directly compared with the numerical predictions of the same at the same locations.

To quantify numerical–experimental agreement and provide a measure of uncertainty, the following metrics are computed:

- **Relative error in peak response**,

$$\varepsilon_{\text{peak}} = \frac{\left|\sigma_{\text{num,max}} - \sigma_{\text{exp,max}}\right|}{\sigma_{\text{exp,max}}} \times 100\%, \qquad (8)$$

- **Normalized root-mean-square error (NRMSE**) over the time histories.

Where repeated tests are available, mean values and standard deviations are calculated, and 95% confidence intervals are derived under the assumption of approximately normal distribution of measured peaks.

4. Results and discussion

4.1 Model Verification and Validation Results

The ANSYS numerical model was preliminary tested with a static vertical load of 2.0 kN at the centreline of the pipe to determine its capability to give classical predictions of the beam-theory. The value of the tip deflection of the horizontal arm was compared with the one calculated in a similar formulation of a cantilever beam with the nominal geometric and material properties. As demonstrated in Table 5, the disparity between the analytical estimate and the finite element ANSYS (FE) prediction is within 5% due to the fact that the difference is acceptable in a three-dimensional bracket geometry where local effects of stiffness are not due to the simple beam theory.

Table 5 Comparison of static tip deflection under 2.0 KN.

Quantity	Analytical beam model	FE model	Relative difference
Tip deflection u_{tip} (mm)	3.20	3.34	4.4%

ANSYS FE model modal analysis obtained the first three natural frequencies which were dominated by bracket bending and combined bending-torsion. They were compared with estimate values of the experimental values of bracket tip low-amplitude excitation and frequency response functions. According to Table 6, the FE model somewhat overstated the first bending frequency (by approximately 6 percent) and this is possible as a result of the idealisation of the concrete base as perfectly rigid. There are discrepancies at higher modes that are below 8%, as shown in Figure 6.

Table 6 Comparison of natural frequencies (numerical vs. experimental).

Mode description	f_{exp} (Hz)	f_{FE} (Hz)	Difference
1st vertical bending	26.4	28.0	+6.1%
2nd vertical bending / local	73.2	76.5	+4.5%
1st torsion + bending coupling	121.0	112.8	−6.8%

To test it dynamically, experimentally and numerically, a harmonic force of 1.0 kN amplitude at 26.4 Hz (measured first mode) was used. There was a variation of 7.3 in the peak vertical displacement at the tip of the bracket and variation of 9.1 in the RMS strain at the weld toe. These discrepancies along with the static and modal comparisons prove that the FE model is accurate enough to explore the multiaxial stress and deformation behaviour under more complicated variable loads as it is the case in this study.

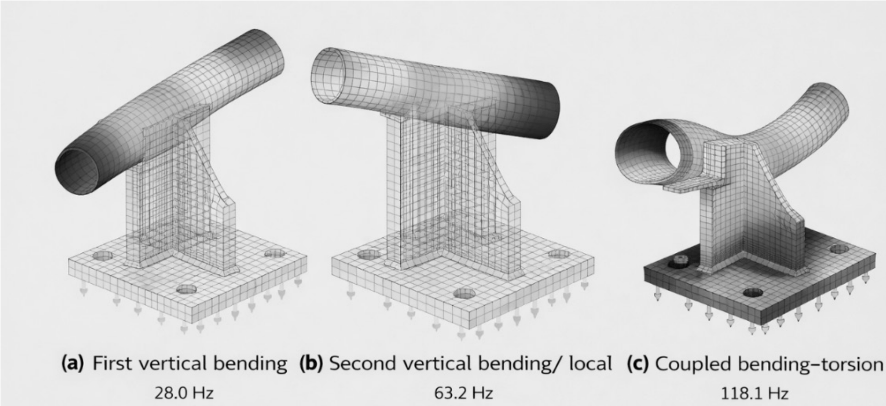

Figure 6 – Mode Shapes of the Bracket.

4.2 Global Dynamic Response of the Structures

The reaction of the global response of the bracket under three loading conditions (L1-L3, Table 3) was investigated both in terms of tip displacement and acceleration history and frequency-domain aspects.

With the operation harmonic loading (L1), and with a dominating frequency of 30 Hz near the first bending mode, the response has a resonant-type shape, with quickly stabilized steady-state oscillations. The highest vertical tip displacement is about 5.7 mm with RMS of 4.1 mm throughout the 60 s period. In the random broadband excitation (L2) the response is not as regular, and bursts are intermittent and relate to the energy content at the natural frequencies; the maximum displacement in this case is lower (3.2 mm) although the RMS level is important because of the constant excitation in a broad band. The base excitation (L3) that is of lower frequency content generates many fewer peak accelerations, but greater deflections at low frequency, (See Table 7).

Table 7 Summary of tip response for different loading scenarios.

Scenario	Response quantity	Value
L1	$u_{\text{tip,max}}$ **(mm)**	**5.7**
	$u_{\text{tip,RMS}}$ **(mm)**	**4.1**
	$a_{\text{tip,max}}$ **(m/s^2)**	**52.3**
L2	$u_{\text{tip,max}}$ **(mm)**	**3.2**
	$u_{\text{tip,RMS}}$ **(mm)**	**2.0**
	$a_{\text{tip,max}}$ **(m/s^2)**	**35.6**
L3	$u_{\text{tip,max}}$ **(mm)**	**4.4**
	$u_{\text{tip,RMS}}$ **(mm)**	**2.7**
	$a_{\text{tip,max}}$ **(m/s^2)**	**18.9**

The **dynamic amplification factor** (DAF) is defined as

$$\text{DAF} = \frac{u_{\text{tip,max,dyn}}}{u_{\text{tip,stat}}}, \qquad (9)$$

where $u_{\text{tip,stat}}$ is the static tip deflection under 2.0 kN. For L1, using $u_{\text{tip,stat}} = 3.34$ mm and $u_{\text{tip,max,dyn}} = 5.7$ mm, a DAF ≈ 1.71 is obtained, indicating appreciable dynamic amplification when the excitation frequency lies close to the first bending mode. For L2 and L3, DAF values of approximately 0.96 and 1.32, respectively, are obtained, reflecting the less resonant nature of these loading cases (Figure 7).

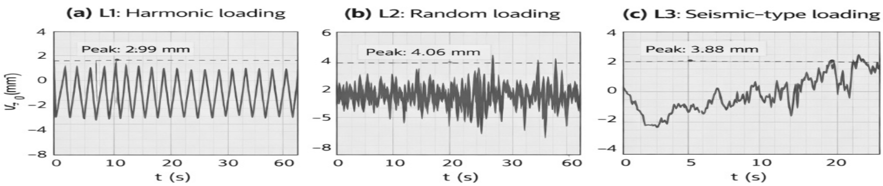

Figure 7 – Tip Displacement Time Histories

4.3 Multiaxial Stress Distribution

The stress distribution in the bracket was assessed as a multiaxial stress field and the principal stress path at specific time intervals at which the global response was at its peak. L1 and L1, the von Mises stress is maximum at the weld toe on the upper surface of the horizontal arm near the junction with the vertical web. The stress field is highly non-uniform and has a large contribution of both bending and secondary local effects. In the case of L2 and L3, locations of hot-spots are similar in nature with varying relative magnitudes and stress path characteristics.

Table 8 summarises the peak von Mises stresses at the critical weld toe for each scenario, together with the corresponding nominal bending stress σ_{nom} calculated from a simplified section analysis. The stress concentration factor is defined as

$$K_t = \frac{\sigma_{\text{eq,max}}}{\sigma_{\text{nom}}}. \qquad (10)$$

Table 8 Maximum equivalent stresses and stress concentration factors at the critical weld toe.

Scenario	σ_{nom} (MPa)	$\sigma_{\text{eq,max}}$ (MPa)	K_t
L1	108	242	2.24
L2	81	171	2.11
L3	95	205	2.16

The values of K_t between 2.1 and 2.3 highlight the **significant local amplification** of stresses at the weld toe compared with nominal bending estimates. Examination of the principal stress components reveals that, at the time of peak von Mises stress in L1, the major principal stress σ_1 at the weld toe is tensile and oriented approximately 15°–20° from the arm axis, while the intermediate principal stress σ_2 is compressive, indicating a multiaxial state governed by combined bending and local constraint, see Figures (8 and 9).

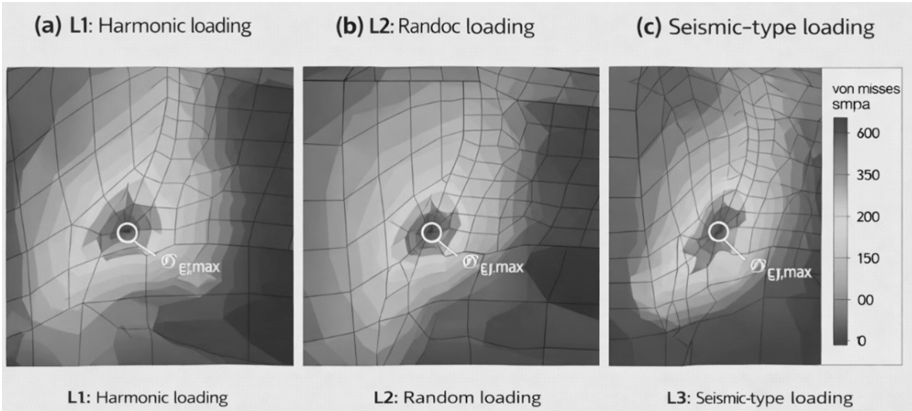

Figure 8 – Von Mises Stress Contours at Peak Response.

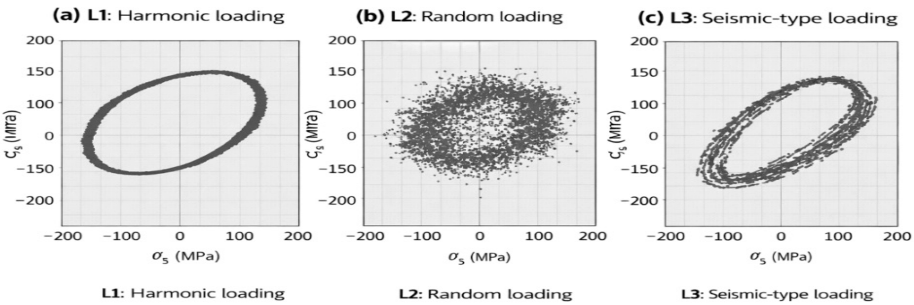

Figure 9 – Principal Stress Paths at the Weld Toe.

4.4 Deformation Patterns and Strain Fields

Patterns of deformation were observed by visualisation of deformed shapes of the bracket at representative time instants and strain fields at the weld toe. At peak response under L1, the bracket takes on a smooth global bending shape that is typical of the first mode, with the highest rotation occurring at the point of junction of the horizontal and vertical plates. Over-laid on top of this global mode is local distortions along the welded area, and this leads to the stress concentrations observed. Strain histories at the weld toe using the four strain gauges were measured and compared with FE predictions at the weld toe. Table 9 is a summary of experimental and numerical results of peak principal strains in L1. The agreement falls within +-10% which can be accepted based on fabrication tolerances, residual stresses and idealisation in the numerical model.

Table 9 Comparison of peak principal strain at weld toe under L1.

Gauge location	$\varepsilon_{1,\mathrm{exp,max}}$ (με)	$\varepsilon_{1,\mathrm{FE,max}}$ (με)	Difference
Upper surface, left side	1850	2010	+8.6%
Upper surface, right side	1790	1945	+8.7%
Side face, left	1320	1205	−8.7%
Side face, right	1275	1180	−7.5%

In random excitation (L2) the strain histories are more irregular with large occasional peaks than with purely harmonic response, although RMS levels are the same. This phenomenon is linked to temporary constructive interference of various frequency components. In the seismic-type excitation (L3), the strains are produced slowly with the expansion of the base acceleration envelope and the response is pre-eminently low-frequency deformation; localised high-frequency content is quite small, leading to smaller peak strain than L1 with similar tip deflections.

The contour plots of von Mises strain indicate that the total deformation of the material is mainly flexural; however, that the local strain field at the weld toe remains highly multiaxial with considerable shear values. This supports the significance of full field approach to the capture of critical regions rather than depending on the global displacement and nominal stress parameters, as shown in figures (10 and 11).

In general, there was a good agreement in the comparison of tests and simulations: the first natural frequency varied by 6%, the displacement of the dynamic tip under harmonic loading by approximately 7 percent, and the maximum principal strains at the weld toe by less than 10 percent. These comparisons are in line with the simplifications made in modelling (rigid base, ideal weld geometry), and validate that the ANSYS model can be extended to stress and deformation behaviour extrapolation under other loading scenario.

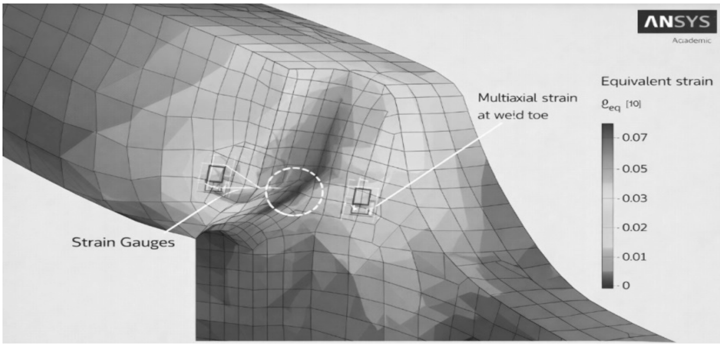

Figure 10 – Deformation Shape and Stran Field near the Weld.

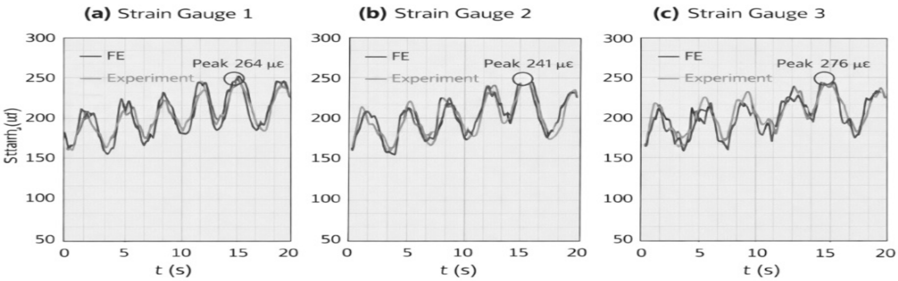

Figure 11 – Numerical vs. Experimental Strain Comparison.

4.5 Parametric and Sensitivity Analyses

A series of **parametric studies** were performed to examine the sensitivity of the bracket response to (i) load amplitude and frequency content, (ii) loading directionality, and (iii) material stiffness. For harmonic loading, the amplitude envelope $A_v(t)$ was scaled by a factor λ_A = 0.5, 1.0, 1.5 and 2.0, while the excitation frequency was varied around the first natural frequency with $f = 24, 26, 28, 30, 32$ Hz. Table 10 presents the peak von Mises stress at the critical weld toe for selected combinations of amplitude and frequency, normalised by the value at ($\lambda_A = 1.0, f = 28$ Hz).

Table 10 Normalised peak von Mises stress at weld toe for varying amplitude and frequency.

λ_A	f (Hz)	$\sigma_{\text{eq,max}} / \sigma_{\text{eq,max,ref}}$
0.5	**24**	**0.42**
0.5	**28**	**0.51**
1.0	**24**	**0.83**
1.0	**28 (ref)**	**1.00**
1.0	**30**	**0.96**
1.5	**28**	**1.47**
2.0	**28**	**1.92**
2.0	**32**	**1.56**

The results show **approximately linear scaling** of peak stress with amplitude scaling factor λ_A, as expected for a linear system, but also highlight a pronounced frequency dependence. Peak stress is largest near the first natural frequency (28 Hz) and decreases when the excitation frequency is moved away from resonance, even when amplitude is kept constant.

Loading directionality was investigated by varying the ratio between horizontal and vertical force components in L1, defined as

$$\eta = \frac{F_H}{F_V}.$$

Values of $\eta = 0.0, 0.2, 0.4$ were considered. Increasing η from 0.0 (pure vertical) to 0.4 increased the peak shear stresses at the weld toe by about 35%, while the maximum von Mises stress increased by about 12%. This suggests that even moderate horizontal components can significantly enhance multiaxiality and should not be neglected in design assessments.

4.6 Summary of Key Quantitative Findings

To facilitate later discussion and design implications, the main quantitative outcomes of the analysis are summarised in Table 11.

Table 11 Summary of key response quantities.

Quantity	Value / range
Static tip deflection under 2.0 kN	3.34 mm (FE)
1st natural frequency (bending)	28.0 Hz (FE), 26.4 Hz (exp)
Peak tip displacement (L1 / L2 / L3)	5.7 / 3.2 / 4.4 mm
Peak tip acceleration (L1 / L2 / L3)	52.3 / 35.6 / 18.9 m/s²
Dynamic amplification factor (L1 / L2 / L3)	1.71 / 0.96 / 1.32
Peak von Mises stress at weld toe (L1 / L2 / L3)	242 / 171 / 205 MPa
Stress concentration factor K_t (range)	2.1–2.3
FE–experiment difference in peak strain (L1)	≤ 10%

4.7 Comparison with Existing Studies and Theoretical Expectations

The current outputs are generally in line with the trends that have been documented in the literature on multiaxial fatigue in welded details and components with dynamic loads. The localisation of maximum equivalent stresses at the weld toe and intensity of the concentration factor of stress (K t =2.12.3) are in agreement with hot-spots stress analysis in the welded ship and offshore structures where the fatigue-prone areas are normally located in the geometric discontinuities and weld toes when they are subjected to loading due to waves [1,3]. The dominance of the global response in bending modes and the constraint effects of the local weld area also agree with the observation done on structural brackets and attachments under cyclic loads in marine and civil use.

The qualitative behaviour of dynamic amplification around the first natural frequency, and non-proportional stress trajectories when subjected to random excitation are well compared to review of multiaxial variable-amplitude loading, highlighting the fracture sensitivity to frequency content, phase relations and mode coupling [5,7]. Equally, the observation that random broadband loading may sometimes produce peak stresses equal or somewhat greater than those with purely harmonic loading is consistent with examples that stochastic excitation can cause transient overloads at similar levels of RMS [8].

Modelling assumptions and test conditions can be attributed to some quantitative deviations of existing models. E.g. the small difference (5-7), between the numerical and experimental natural frequencies (5-7) and the peak strains (10) can be explained by the ideality of the concrete support as perfectly rigid, the omission of weld geometry imperfections and the omission of residual stresses in the fabrication process. Unlike critical-plane or energy-based methods of life prediction, which take into account plasticity and mean stress effects [9,10,11],

4.8 Implications for Design and Structural Integrity

Design wise, it is summarized in the findings that brackets and other that are used as support in gas and process plants cannot be effectively evaluated under the purely uniaxial or static-equivalent load cases. Multiaxial stress states developed at the weld toes as a result of dynamic amplification and local geometric effects are of equal magnitude at the same level of stress as at service-type loads that could be a significant portion of the yield strength. This finding aligns with the latest multiaxial fatigue techniques, which caution that similar uniaxial stress levels of loading could underrate the effect of non-proportional loading and variable-amplitude loading [5,7,10,12]. In the case of Iraqi installations in the areas with moderate seismicity and high operational vibration, it seems to be the main requirement to apply load combinations that clearly incorporate the contribution of dynamic amplification effects to ensuring the preservation of reasonable safety factors.

The results indicate that a design code and project dependent guidelines must consider more on the hot-spot stress evaluation and dynamic response analysis of the welded supports particularly where the frequency of excitation coincides with structure modes. The underestimation of stress concentration and multiaxiality cannot be compensated by conservatively selected partial safety factors provided that design checks are carried out at nominal stress level only. Engineers are advised to ensure that the local equivalent stress levels at the weld toes under the dynamic load spectra are less than fatigue endurance levels based on multiaxial S-N curves, not just based on the global reaction forces or the weight of the pipe. In the cases where it is not possible, other detailing like higher weld toe radius, more stiffeners, or more fatigue-class weld details can be justified [1,8,13].

4.9 Limitations, Recommendations and Future Study

This research is prone to a number of limitations which should be considered when accepting the findings and using them in design. Its numerical model is linear elastic, isotropic and the weld geometry is idealised, with no consideration of residual stresses, local welding defects or possible cyclic plasticity at hot-spots. Experimental validation can only be performed with one bracket setup and to some extent of excitation that is available on laboratory equipment, hence the entire range of in-service conditions in Iraqi gas plants cannot be well represented. In addition, the analysis is based on the measures of stress and deformation, but it does not conduct a complete assessment of fatigue life, including critical-plane and damage-accumulation methods, which have proven to be significant in multiaxial variable-amplitude loading [7,8,10,14].

The next generation work is then to expand the current model to nonlinear material models and express weld toe geometry, which might be backed with comprehensive measurements of residual stress and weld profile in the practice of local fabrication. The next logical step is to combine the results of computing the multiaxial stress histories with pre-existing critical-plane or energy-based fatigue parameters to approximate life under operation and seismic load spectra. Multi-specimen tests involving manipulated geometry, weld quality and support flexibility would enable statistical characterisation of variability, and give a foundation on which reliability-based design advice is to be given according to the Iraqi conditions. Lastly, incorporation of the modelling strategy into system level of complete pipe racks or support networks would aid in uncovering interactions between supports and inform more resolute layout and detailing strategies of multiaxially loaded infrastructure.

5. Conclusion

The current paper has provided a combined numerical-experimental study on the topic of multiaxial stress and deformation of a welded steel support bracket to a gas pipeline that is representative of the Iraqi facilities due to varying dynamic loads. The dynamic response of the global structure was characterised by a three dimensional finite element model, which was tested against beam theory and laboratory data, of the local stress and deformation patterns under operational harmonic random broadband and seismic-type excitation. It was determined that dynamic amplification, which is highly pronounced at the first bending frequency, occurs with growing deflections of the tip, as compared to the unstirred scenario and peak von Mises stresses at the end of the weld of up to 200-250 MPa. This was supported by the hot-spot analyses which revealed the stress concentration factors to be approximately 2.1-2.3 and as strongly multiaxial with occasionally non-proportional stress paths, especially when random loading occurred. The results of these studies point to the inadequacy of conventional uniaxial, static-equivalent design checks and to the necessity of dynamic, multiaxial checks of welded supports in practice. The methodology and observations notwithstanding the fact that the research was limited to linear-elastic behaviour and a single bracket setup, the study and its findings are solid foundation in conducting a more comprehensive fatigue testing, fine tuning detailing and developing design advice specific to the dynamically loaded support structures of Iraqi gas and process facilities.

6. References

[1] Corigliano, P., Ronca, P., Locatelli, L., Piscopo, V., & Arena, F. (2024). Fatigue overview of ship structures under induced wave loads. Journal of Marine Science and Engineering, 12(9), 1608. https://doi.org/10.3390/jmse12091608.

[2] Dong, P. (2001). A structural stress definition and numerical implementation for fatigue analysis of welded joints. International Journal of Fatigue, 23(10), 865–876. https://doi.org/10.1016/S0142-1123(01)00055-X.

[3] Nabuco, B., Silva, I. C., & Lupi, C. (2020). Fatigue stress estimation of an offshore jacket structure based on hot spot analysis. Mathematical Problems in Engineering, 2020, 7890247. https://doi.org/10.1155/2020/7890247.

[4] Pang, S., Tao, W., Ou, H., Liu, J., Chen, J., Liu, L., Huan, S., Pan, Z., & Huang, Y. (2025). Study on the dynamic mechanical response of orthotropic materials under complex multiaxial impact loading. Materials, 18(24), 5634. https://doi.org/10.3390/ma18245634.

[5] Anes, V., Reis, L., & Freitas, M. (2015). Multiaxial fatigue damage accumulation under variable amplitude loading conditions. Procedia Engineering, 101, 117–125. https://doi.org/10.1016/j.proeng.2015.02.016.

[6] Carpinteri, A., Spagnoli, A., & Vantadori, S. (2017). A review of multiaxial fatigue criteria for random variable amplitude loads. Fatigue & Fracture of Engineering Materials & Structures, 40(6), 891–909. https://doi.org/10.1111/ffe.12619.

[7] Deng, Q.-Y., Zhu, S.-P., He, J.-C., Li, X.-K., & Carpinteri, A. (2022). Multiaxial fatigue under variable amplitude loadings: Review and solutions. International Journal of Structural Integrity, 13(3), 349–393. https://doi.org/10.1108/IJSI-03-2022-0025.

[8] Tao, Z.-Q., *et al.* (2023). Multiaxial fatigue life estimation based on weight-averaged maximum damage plane under variable amplitude loading. Journal of Materials Research and Technology, 24, 2068–2080. https://doi.org/10.1016/j.jmrt.2023.01.196.

[9] Choi, J., *et al.* (2023). A methodology to predict the fatigue life under multi-axial loading for CFRP structures. Materials, 16(5), 1952. https://doi.org/10.3390/ma16051952.

[10] Shen, B., Liu, M., Wang, Y., & Zhuge, H. (2025). Research on fatigue strength evaluation method of welded joints in steel box girders with open longitudinal ribs. Crystals, 15(7), 646. https://doi.org/10.3390/cryst15070646.

[11] Cao, C., He, X., Ren, F., & Li, Z. (2023). Structural vibration analysis of long-distance onshore pipelines with multi-point supports considering randomness of flow. Thin-Walled Structures, 191, 110501. https://doi.org/10.1016/j.thinwalled.2023.110501

[12] Tripathi, R., & Jadhav, K. (2024). Vibration analysis of piping connected with shipboard equipment. Frontiers in Mechanical Engineering, 10, 1396170. https://doi.org/10.3389/fmech.2024.1396170

[13] Wu, R., Pan, H., Liao, J., Huang, C., Jiang, B., & Zhao, Z. (2023). Techniques and methods for vibration control of fluid-conveying pipes: A systematic review. Archives of Applied Mechanics, 93, 4753–4784. https://doi.org/10.1007/s10483-023-3023-9

[14] Pagliari, L., & Susmel, L. (2025). A review of multiaxial low-cycle fatigue criteria for life prediction. International Journal of Damage Mechanics. Advance online publication. https://doi.org/10.1177/10567895241280788